IEEE Access
Multidisciplinary ⋮ Rapid Review ⋮ Open Access Journal

Received August 17, 2018, accepted September 25, 2018, date of publication October 8, 2018, date of current version December 18, 2018.

Digital Object Identifier 10.1109/ACCESS.2018.2873709

Dynamics Modeling of a Wave Glider With Optimal Wing Structure

JIAWANG CHEN, YONGQIANG GE, CHAOLING YAO, AND BINGHUAN ZHENG
Ocean College, Zhejiang University, Zhoushan 316021, China

Corresponding author: Jiawang Chen (arwang@zju.edu.cn)

This work was supported by the Zhejiang Conservation Science and Technology Program of Administration of Cultural Heritage, China, under Grant 2016010.

ABSTRACT The wave glider is a new concept marine robot that can make use of wave energy to obtain thrust. Differ from the traditional unmanned vehicle, the wave glider consists of the floating body, the connecting tether, and the submerge glider. It can be regarded as a special catamaran structure. Therefore, the conventional kinetic models of the unmanned vehicle are inapplicable to the wave glider. In this paper, we propose a non-linear kinetic model of wave glider of six degrees of freedom based on three reference coordinate frames. The calculating formula between the vertical liquid velocity and the system advance speed is derived by using the kinetic model. A method to design a glider wing structure under fixed wave speed in vertical direction was also presented. On the basis of the static stress analysis of the Glider wings, we compare different factors influencing the advance speed and optimize them by comparing the simulation results with the calculation results.

INDEX TERMS Wave glider, kinetic model, marine vehicles, catamaran structure.

NOMENCLATURE OF ALL STATE VARIABLES

Name	Description
$\boldsymbol{G}^{\boldsymbol{0}}$	Weight of the system
$\boldsymbol{G}^{\boldsymbol{F}}$	Weight of the floater
$\boldsymbol{B}^{\boldsymbol{0}}$	Buoyancy of the system
$\boldsymbol{B}^{\boldsymbol{F}}$	Buoyancy of the floater
M	Inertia matrix
C/c	Matrix of centripetal force and Coriolis force
D/d	Damping matrix
g	Vector of gravitational forces and moments
τ	Vector of control inputs
η	Position and Euler angle states (Earth-fixed frame)
ν	Velocity and Euler angle rate states (body-fixed)
$\boldsymbol{x}^{\boldsymbol{0,F,G}}$	X-position of the center of system, floater, and glider, the superscript represents the corresponding moving component
$\boldsymbol{y}^{\boldsymbol{0,F,G}}$	Y-position of the center of system, floater, and glider, the superscript represents the corresponding moving component
$\boldsymbol{z}^{\boldsymbol{0,F,G}}$	Z-position of the center of system, floater, and glider, the superscript represents the corresponding moving component
$\boldsymbol{\Phi}^{\boldsymbol{0,F,G}} = \Phi$	Rotation over roll angle Φ about X of system, floater, and glider
$\boldsymbol{\theta}^{\boldsymbol{0,F,G}} = \theta$	Rotation over pitch angle θ about Y of system, floater, and glider
$\boldsymbol{\psi}^{\boldsymbol{0,F,G}}$	Rotation over heading angle ψ about Z of system, floater, and glider
$\Delta\psi$	Difference between floater and glider heading
δ	Angle of the tether
$\boldsymbol{u}^{\boldsymbol{0,F,G}}$	Surge velocity of system, floater and glider (along x-axis)
$\boldsymbol{v}^{\boldsymbol{0,F,G}}$	Sway velocity of system, floater and glider (along y-axis)
$\boldsymbol{\omega}^{\boldsymbol{0,F,G}}$	Heave velocity of system, floater and glider (along z-axis)
$\boldsymbol{p}^{\boldsymbol{0,F,G}}$	Roll rate of system, floater and glider (around the x-axis).
$\boldsymbol{q}^{\boldsymbol{0,F,G}}$	Pitch rate of system, floater and glider (around the y-axis).
$\boldsymbol{r}^{\boldsymbol{0,F,G}}$	Yaw rate of system, floater and glider (around the z-axis).
$\boldsymbol{E}_{\boldsymbol{xyz}}$	Earth-fixed coordinate system
$\boldsymbol{F}_{\boldsymbol{xyz}}$	Body-fixed coordinate system of the floater

O_{xyz}	Body-fixed coordinate system of the system
$X_{\dot{u}}^{O,F,G}$	Added mass caused by advance and retreat movement, the superscript represents the corresponding moving component
$Y_{\dot{v}}^{O,F,G}$	Added mass caused by traverse movement, the superscript represents the corresponding moving component
$N_{\dot{r}}^{O,F,G}$	Added inertia caused by trim movement, the superscript represents the corresponding moving component
$m^{0,F,G}$	Weight of each part, the superscript represents the corresponding moving component
$I_{zz}^{0,F,G}$	Rotary inertia of each part around Z-axis, the superscript represents the corresponding moving component
$\|r_{F0}\|$	Distance from the floater's center of gravity to the center of gravity of the entire system
$\|r_{G0}\|$	Distance from the Glider wings' center of gravity to the center of gravity of the entire system
X_T^G	Thrust in X-direction generated by the wings
$X_{u\delta}^G(\delta)$	Thrust in X-direction generated by the rudder angle
Y_T^G	Thrust in Y-direction generated by the wings
$Y_{u\delta}^G(\delta)$	Thrust in Y-direction generated by the rudder angle
$N_{uu\delta}^G$	Rotary inertia around Z-axis generated by the Glider wings below
X_u^F	Damping force in X-axis direction on the center of gravity of the system caused by the advance and retreat movement of the floater
X_v^F	Damping force in X-axis direction on the center of gravity of the system caused by the traverse movement of the floater
X_u^G	Damping force in X-axis direction on the center of gravity of the system caused by the advance and retreat movement of Glider wings
X_v^G	Damping force in X-axis direction on the center of gravity of the system caused by the traverse movement of Glider wings
Y_u^F	Damping force in y-axis direction on the center of gravity of the system caused by the advance and retreat movement of the floater
Y_v^F	Damping force in y-axis direction on the center of gravity of the system caused by the traverse movement of the floater
Y_u^G	Damping force in y-axis direction on the center of gravity of the system caused by the advance and retreat movement of Glider wings
Y_v^G	Damping force in y-axis direction on the center of gravity of the system caused by the traverse movement of Glider wings

I. INTRODUCTION

Since 1993, the ASC (Autonomous Surface Craft) was developed. At the same time, the ARTEMIS was designed as a precision survey platform at the MIT Sea Grant College Program [1]. One of the main disadvantages of ARTEMIS is its small size, which limits its applications and durability. In 1997, ARTEMIS was upgraded to ASC ACES (Autonomous Coastal Exploration System) [2], a new waterborne robot which was more durable, stable and easy to deploy. The new waterborne robot had completed field tests off Gloucester, MA during the summer of 1997. Between September 1998 and June 2000, the mechanical systems of the ASC were heavily modified. During the extensive field-testing of ACES several potential improvements in the basic platform design were identified as desirable [2].

After that, the technology of waterborne unmanned robot developed rapidly. With the requirement of long-time and wide-range ocean data, the endurance of waterborne unmanned robot became the research emphasis. People are looking forward to innovating new driving system of the waterborne unmanned robot. In 2005, Roger Hine designed a new marine observation system—the prototype of wave glider, which requires no expensive deep sea mooring but has a strong durability [3]–[6]. In past several years, wave glider has proven its durability and stability in ocean tests and practical applications [7]–[9].

Simultaneous Interaction between Catamaran structures of Wave Glider is similar to operating modes between ROV (Remotely Operated Vehicle) and a ship. A kinetic equation of several degrees of freedom with moving reference coordinate frames is necessary for motion simulation and estimation. In the literature [11], Caiti *et al.* introduced a control-oriented Lagrangian modeling approach for Wave Glider within different reference coordinate frames, including classic Denavit-Hartenberg (DH) convention [26] and North-East-Down (NED) coordinates [21]. However, the literature [11], [12] didn't introduce much detail about the static stress analysis of the Glider wings and therefore hydrodynamic optimization of the wing structure of Wave Glider is poor improved in [11] and [12]. The load-carrying capability of Wave Glider and details about the stress situations of underwater glider wings would also not be introduced in [10]. The kinetic equation of four degrees of freedom also fails to accurately describe the movement of the glider. The relationship between the vertical flow velocity and the speed of the glider has not yet been formulized in the literature [10]–[12].

Based on the special structural characteristics of the glider, this paper describes a non-linear kinetic model of six degrees of freedom (6-DOF) in three reference coordinate frames, including two body-fixed coordinates for catamaran structures estimation, and an Earth-fixed coordinate for observation. In order to simplify the complexity of the coordinate transformation, this model integrates special terms in hydrodynamics with speed of gravity center in advance, retreat and traversing, rates of heeling angle, and advance of hull. In the paper, the static stress situation of the glider wings is analyzed and, the formula between the vertical flow velocity and the speed of the glider is derived.

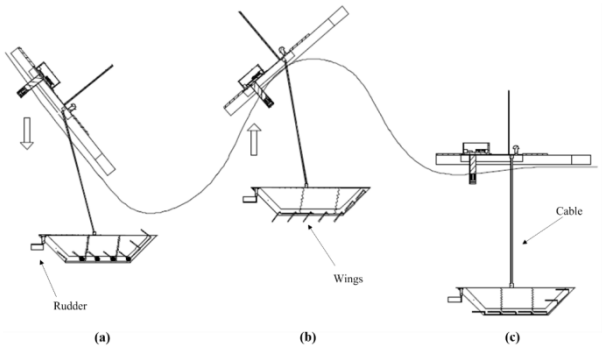

FIGURE 1. Movement mechanism of the wave glider.

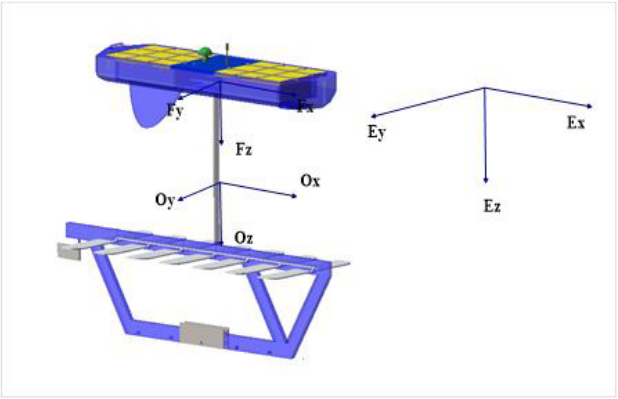

FIGURE 2. Definition of the system coordinate system.

II. DYNAMIC MODELING OF WAVE GLIDER

The wave glider is composed of a submerge glider and a floating body connected by a tether. The wave glider is propelled by converting vertical wave motions into forward thrust using the parallel wings array [13]–[15]. The vertical motion of the wave acts on the parallel wings of the wave glider and then is converted into forward thrust. The overall system is a mechanical-propelled structure, which will not require any external power and consequently is secure and energy saving [16], [17]. The movement mechanism with three operating modes is shown in Fig. 1 (a), (b) and (c). The underwater glider will convert the wave motion into the thrust when the floater moves up and down with the waves. When the floating body encounters the wave crest, the floating body pulls the submerge glider to tighten the tether, as shown in Fig. 1 (b). The parallel wings array rotate downward under the action of water flow from the vertical direction. The water flows downward and acts on the upper surface of the wings array. The horizontal component drag force pushes the glider going forward. When the rotation angle gets to the maximum value, the torsional force will rotate the torsional spring to restore to its original condition. When the floating body encounters the wave valley, the wings of the underwater glider sink due to the gravity, as shown in the Fig. 1 (a). The parallel wings in the submerge glider rotate upward under the action of water flow from the vertical direction. The water flows upward and acts on the lower surface of the wings. When the rotation angle gets to the maximum, the torsional force will rotate the torsional spring to restore to its original condition. The horizontal component force pushes the glider going forward. The overall system moves without any external power [18], [19].

A. ESTABLISHMENT OF COORDINATE SYSTEM

This wave glider consists of two rigid parts: the surface floater and the underwater glider, which are connected by a tether. To describe the movement of the wave glider, we establish three reference frames (Fig. 2): two body-fixed and one Earth-fixed coordinate system. They are defined as follows:

(1) Earth-fixed coordinate system (inertial coordinate system), which is represented by Ex-Ey-Ez;

(2) Floater-fixed coordinate system: Body-centered coordinate system of the floater, the origin is set at the center of gravity of the floater, which is represented by Fx-Fy-Fz;

(3) System-fixed coordinate system: Body-centered coordinate system of the whole system, the origin is set at the center of gravity of the wave glider, which is represented by Ox-Oy-Oz.

The position and angle states of the wave glider are represented by Euler angles using the SNAME notation [23]. $\eta_1 = \left[x^{0,F}, \mathrm{y}^{0,F}, z^{0,F}\right]^T$ denotes the position vector of the system and the floater in the earth-fixed coordinate system(the superscript represents the corresponding part). $\eta_2 = \left[\Phi^{0,F}, \theta^{0,F}, \psi^{0,F}\right]^T$ denotes the orientation vector of the system and the floater in the Earth-fixed coordinate system (the superscript represents the corresponding part). $V_1 = \left[u^{0,F}, v^{0,F}, \omega^{0,F}\right]^T$ denotes the linear speed of the system and the floater in the body-fixed coordinate system (the superscript represents the corresponding part).$V_2 = \left[\mathrm{p}^{0,F}, q^{0,F}, r^{0,F}\right]^T$ denotes the attitude angular speed of the system and the floater in the body-fixed coordinate system (the superscript represents the corresponding part). External force of the whole system is expressed as $\tau_1 = [X, \mathrm{Y}, \mathrm{Z}]^T$, external torque of the system is expressed as $\tau_2 = [K, \mathrm{M}, \mathrm{N}]^T$.

B. TRANSFORMATION OF COORDINATES

In order to obtain the equations of motion in the wave glider system, coordinate transformation between the vectors was executed or carried out. To simplify the coordinate transformations, sin () and cos () are abbreviated as s () and c (), tan () is abbreviated as t (), the super script represents the corresponding moving coordinate system. The linear speed conversion matrix is as follows [20], [21] (1), as shown at the top of the next page:

The angular speed conversion matrix is as follows (excluding the situation when θ=90°):

$$J_2(\eta_2) = \begin{bmatrix} 1 & \mathrm{s}\left(\Phi^{0,F}\right)\mathrm{t}\left(\theta^{0,F}\right) & c\left(\Phi^{0,F}\right)t\left(\theta^{0,F}\right) \\ 0 & \mathrm{c}\left(\Phi^{0,F}\right) & -s\left(\Phi^{0,F}\right) \\ 0 & \mathrm{s}\left(\Phi^{0,F}\right)/\mathrm{c}\left(\theta^{0,F}\right) & c(\Phi^{0,F})/\mathrm{c}\left(\theta^{0,F}\right) \end{bmatrix} \tag{2}$$

$$J_1(\eta_2)=\begin{bmatrix} c(\psi^{O,F})c(\theta^{O,F}) & -s(\psi^{O,F})c(\phi^{O,F})+c(\psi^{O,F})s(\theta^{O,F})s(\phi^{O,F}) & s(\psi^{O,F})s(\phi^{O,F})+c(\psi^{O,F})c(\phi^{O,F})s(\theta^{O,F}) \\ s(\psi^{O,F})c(\theta^{O,F}) & c(\psi^{O,F})c(\phi^{O,F})+c(\phi^{O,F})c(\theta^{O,F})s(\psi^{O,F}) & -c(\psi^{O,F})s(\phi^{O,F})+s(\theta^{O,F})s(\psi^{O,F})c(\phi^{O,F}) \\ -s(\theta^{O,F}) & c(\theta^{O,F})s(\phi^{O,F}) & c(\theta^{O,F})s(\phi^{O,F}) \end{bmatrix} \tag{1}$$

The relationship between the linear speed in the inertial coordinate system and the linear speed in the moving coordinate system is $\dot{\eta_1} = J_1(\eta_2)V_1$; the relationship between the angular speed in the inertial coordinate system and the angular speed in the moving coordinate system is $\dot{\eta_2} = J_2(\eta_2)V_2$, the overall relationship is as follows:

$$\begin{bmatrix} \cdot \\ \eta_1 \\ \cdot \\ \eta_2 \end{bmatrix} = \begin{bmatrix} J_1(\eta_2) & 0 \\ 0 & J_2(\eta_2) \end{bmatrix} \begin{bmatrix} V_1 \\ V_2 \end{bmatrix} \tag{3}$$

Namely $\dot{\eta} = \mathrm{J}\ (\eta)\ \mathrm{V}$

Assumptions in this model: the entire tether is assumed to be stretched straight (this assumption is invalid in extreme weather), the weight of the tether is negligible; the floater has always been floating on the sea surface, and the glider is assumed to always pull the floater so the tether is always in tension. The displacement of the whole glider in Z-axis direction is very small, accordingly disregarded in this study. The center of gravity of the entire wave glider is on the cable, the movement at the center of gravity is approximately the same with that of the fins of the glider. Each coordinate system origin is located at the C.G. of its corresponding body. In particular, the yaw of the wave glider system is equal to the yaw of the glider [22]

Each of the two body-fixed coordinate systems established in this paper has 6 state variables, so there are a total of 12 state variables, among which are not all considered. They respectively are surge speed of the wave glider system u^0, sway speed of the wave glider system v^0, yaw speed of the wave glider system r^0, surge speed of the floater u^F, sway speed of the floater v^F, yaw speed of the floater r^F, namely $\eta = \left[x^0, y^0, \psi^0, x^F, y^F, \psi^F\right]^T$ (yaw angle of the wave glider system ψ^0 is assumed to be approximately the same with the yaw angle of the blades ψ^G), $\mathrm{V} = \left[u^0, v^0, \mathrm{r}^0, u^F, v^F, r^F\right]^T$. Hence, the rates in pitch, roll and heave of the floater and the system are not considered in this model.

C. KINETIC MODELING OF WAVE GLIDER

In order to describe the dynamic characteristics of the entire wave glider system, we use T. I. fossen's nonlinear model [21]. The 6-DOF set of non-linear equations of motion for the wave glider can be expressed as follows:

$$\mathrm{M}\dot{\mathrm{V}} + \mathrm{C(V)V} + \mathrm{D(V)} + \mathrm{g}(\eta) = \tau \tag{4}$$

In the model above, $\mathrm{M} = \mathrm{M}_{RB} + \mathrm{M}_A$, $\mathrm{C(V)} = \mathrm{C}_{RB}(\mathrm{V}) + \mathrm{C}_A(\mathrm{V})$, M_{RB} is the inertia matrix, M_A is the additional mass and inertia matrix, $\mathrm{C}_{RB}(\mathrm{V})$ is the Coriolis and centripetal matrix, $\mathrm{C}_A(\mathrm{V})$ is the hydrodynamic Coriolis and centripetal matrix, D(V) is the damping matrix, g(η) is the restoring forces and moments vector, τ is the control input vector.

The M_A is estimated using the strip theory [6]. For added mass of glider wings, the interactions between the wings and the impact from the floater are not considered. Due to the computational complexity of their values, the off-diagonal cross terms of the inertia matrix are not considered. The floater structure is approximately symmetric on X-axis and Y-axis, and the off-diagonal terms of the inertia matrix are approximated to zero. Inertia matrix M is simplified as follows (5), as shown at the top of the next page:

The above formula,m^0, m^G and m^F represent the mass of overall wave glider system, the mass of glide wings and the mass of the floater respectively; we have $\mathrm{m}^0 = \mathrm{m}^\mathrm{G} + \mathrm{m}^\mathrm{F}$. The I^0_{zz} and $\mathrm{I}^\mathrm{F}_{zz}$ represent the yaw moments of inertia of the entire system and the floater around Z-axis respectively; $\mathrm{X}^\mathrm{G}_{\dot{u}}$,$\mathrm{X}^\mathrm{F}_{\dot{u}}$, $\mathrm{Y}^\mathrm{G}_{\dot{v}}$, $\mathrm{Y}^\mathrm{F}_{\dot{v}}$, $\mathrm{Y}^\mathrm{G}_{\dot{r}}and\mathrm{Y}^\mathrm{F}_{\dot{r}}$ represent additional mass forces from different directions of the glider and the floater wings respectively; $N^0_{\dot{v}}$, $N^0_{\dot{r}}$, $N^F_{\dot{v}}$, and$N^\mathrm{F}_{\dot{r}}$ represent the added moments of inertia of the system and the floater around Z-axis. According to the strip theory, the calculation of the added mass force and added moment inertia is derived based on the empirical formula [23] as in (6) to approximate the surface of the floater to a cylinder.

$$\mathrm{X}_{\dot{u}} = -\frac{4\alpha\rho\pi}{3}\left(\frac{\mathrm{L}}{2}\right)\left(\frac{\mathrm{d}}{2}\right)^2 \tag{6}$$

Where α is the empirical coefficient calculated through the length-diameter ratio, ρ is the fluid density, L represents the length in X direction, d is radius of the approximate cylinder. Because of the special structure of the underwater Glider wings, the formula cannot be directly used, the added mass coefficient of a single wing shall be calculated first, the added mass coefficient of the entire glider is derived through the addition of every $X^G_{\dot{u}}$. The remaining parameters are calculated as follows:

$$Y_{\dot{v}} = -\int_{-L/2}^{L/2} \pi\rho \mathrm{R(x)}^2 dx \tag{7}$$

$$N_{\dot{v}} = Y_{\dot{r}} = -\int_{-L/2}^{L/2} \pi\rho x \mathrm{R(x)}^2 dx \tag{8}$$

$$N_{\dot{r}} = -\int_{-L/2}^{L/2} \pi\rho x^2 \mathrm{R(x)}^2 dx \tag{9}$$

Where R(x) is the function of radius and position x, when the floater is approximated as a cylinder.

The maximum design forward speed of the entire system is 1.5 knot (0.77m/s), the total mass is 75 kg (calculated based on the prototype) in north latitude 30° as the experimental

$$
\begin{aligned}
\mathrm{M} &= \mathrm{diag}\left\{\mathrm{m}_{11}^{0}, \mathrm{m}_{22}^{0}, \mathrm{m}_{33}^{0}, \mathrm{m}_{44}^{\mathrm{F}}, \mathrm{m}_{55}^{F}, \mathrm{m}_{66}^{F}\right\} \\
\mathrm{m}_{11}^{0} &= \mathrm{m}^{0} + X_{\dot{u}}^{G} + X_{\dot{u}}^{F} \\
\mathrm{m}_{22}^{0} &= \mathrm{m}^{0} + Y_{\dot{v}}^{G} + Y_{\dot{v}}^{F} \\
\mathrm{m}_{33}^{0} &= I_{zz}^{0} + N_{\dot{r}}^{0} \\
\mathrm{m}_{44}^{F} &= \mathrm{m}^{F} + X_{\dot{u}}^{F} \\
\mathrm{m}_{55}^{F} &= \mathrm{m}^{F} + Y_{\dot{v}}^{F} \\
\mathrm{m}_{66}^{F} &= I_{zz}^{F} + N_{\dot{r}}^{F} \\
\mathrm{M}_{RB} &= \begin{bmatrix} \mathrm{m}^{0} & 0 & 0 & 0 & 0 & 0 \\ 0 & \mathrm{m}^{0} & 0 & 0 & 0 & 0 \\ 0 & 0 & I_{zz}^{0} & 0 & 0 & 0 \\ 0 & 0 & 0 & \mathrm{m}^{F} & 0 & 0 \\ 0 & 0 & 0 & 0 & \mathrm{m}^{F} & 0 \\ 0 & 0 & 0 & 0 & 0 & I_{zz}^{F} \end{bmatrix} \\
\mathrm{M}_{A} &= \begin{bmatrix} -X_{\dot{u}}^{G} - X_{\dot{u}}^{F} & 0 & 0 & 0 & 0 & 0 \\ 0 & -Y_{\dot{v}}^{G} - Y_{\dot{v}}^{F} & -Y_{\dot{r}}^{G} - Y_{\dot{r}}^{F} & 0 & 0 & 0 \\ 0 & -N_{\dot{v}}^{0} & -N_{\dot{r}}^{0} & 0 & 0 & 0 \\ 0 & 0 & 0 & -X_{\dot{u}}^{F} & 0 & 0 \\ 0 & 0 & 0 & 0 & -Y_{\dot{v}}^{F} & -Y_{\dot{r}}^{F} \\ 0 & 0 & 0 & 0 & -N_{\dot{v}}^{F} & -N_{\dot{r}}^{F} \end{bmatrix}
\end{aligned} \tag{5}
$$

$$
C_{RB}(V) = \begin{bmatrix} 0 & 0 & -\mathrm{m}^{0}v^{0} & 0 & 0 & 0 \\ 0 & 0 & \mathrm{m}^{0}u^{0} & 0 & 0 & 0 \\ \mathrm{m}^{0}v^{0} & -N_{\dot{v}}^{0} & 0 & 0 & 0 & 0 \\ 0 & 0 & 0 & 0 & 0 & -\mathrm{m}^{F}v^{F} \\ 0 & 0 & 0 & 0 & 0 & \mathrm{m}^{F}u^{F} \\ 0 & 0 & 0 & \mathrm{m}^{F}v^{F} & -\mathrm{m}^{F}u^{F} & 0 \end{bmatrix} \tag{10}
$$

$$
C_{A}(V) = \begin{bmatrix} 0 & 0 & Y_{\dot{v}}^{O}v^{O} + Y_{\dot{r}}^{O}r^{O} & 0 & 0 & 0 \\ 0 & 0 & \mathrm{m}^{0}u^{0} & 0 & 0 & 0 \\ -Y_{\dot{v}}^{O}v^{O} - Y_{\dot{r}}^{O}r^{O} & X_{\dot{u}}^{O}u^{O} & 0 & 0 & 0 & 0 \\ 0 & 0 & 0 & 0 & 0 & Y_{\dot{v}}^{F}v^{F} + Y_{\dot{r}}^{F}r^{F} \\ 0 & 0 & 0 & 0 & 0 & -X_{\dot{u}}^{F}u^{F} \\ 0 & 0 & 0 & -Y_{\dot{v}}^{F}v^{F} - Y_{\dot{r}}^{F}r^{F} & X_{\dot{u}}^{F}u^{F} & 0 \end{bmatrix} \tag{11}
$$

estimation conditions, the calculated maximum Coriolis force is 0.01 N, therefore, in $\mathrm{C}_{RB}(\mathrm{V})$, the influence of Coriolis force on the entire system can be ignored. $\mathrm{C}_{RB}(\mathrm{V})$ is simplified to (10) and (11), as shown at the top of this page:

Damping matrix is nonlinear with linear speed and angular speed, which can be expressed as follows:

$$
\begin{aligned}
\mathrm{D(V)} &= \left[X^{0}Y^{0}N^{0}X^{F}Y^{F}N^{F}\right]^{T} \\
X^{0} &= X_{u}^{F} + X_{u}^{G} \\
Y^{0} &= Y_{v}^{F} + Y_{v}^{G} \\
N^{0} &= N_{r}^{F} + N_{r}^{G} \\
X^{F} &= X_{u}^{F} + X_{v}^{F} \\
Y^{F} &= Y_{u}^{F} + Y_{v}^{F} \\
N^{F} &= N_{r}^{F}
\end{aligned} \tag{12}
$$

In the above formula, $X_{u}^{F,\mathrm{G}}$, $Y_{v}^{F,\mathrm{G}}$

$$
X_{u}^{F,\mathrm{G}} = -(\frac{1}{2}\rho c_{d}A_{uf})u\,|u| \tag{13}
$$

$$
Y_{v}^{F,\mathrm{G}} = -(\frac{1}{2}\rho c_{d}A_{vf})v\,|v| \tag{14}
$$

Where ρ represents the liquid density, A_{uf} and A_{vf} represent the effective cross-sectional areas in the speed direction in surge and sway respectively, c_{d} represents the damping coefficient in surge, which is derived according to the empirical formula as [23]:

$$
c_{d} = \frac{c_{\mathrm{ss}}\pi ld}{A_{f}}\left[1 + 60\left(\frac{d}{l}\right)^{3} + 0.0025\left(\frac{d}{l}\right)\right] \tag{15}
$$

The vector of restoring force and moments g(η) are derived from transforming the weight and buoyancy force to the body-fixed coordinate system. Assume that the entire wave glider system and the floater keep neutral buoyancy, i.e., the gravity equal to the buoyancy of entire systems, $G^o = B^o$, and $G^F = B^F$ of the floater. The center of system buoyancy is expressed as $r_B^o = \left[r_{Bx}^o, r_{By}^o, r_{Bz}^o\right]^T$; the center of gravity of the entire system is expressed as $r_{\mathrm{G}}^o = \left[r_{Gx}^o, r_{Gy}^o, r_{Gz}^o\right]^T$; the center of buoyancy of the floater is expressed as $r_B^F = \left[r_{Bx}^F, r_{By}^F, r_{Bz}^F\right]^T$ and the center of gravity of the floater is expressed as $r_{\mathrm{G}}^F = \left[r_{Gx}^F, r_{Gy}^F, r_{Gz}^F\right]^T$. The weight and buoyancy force vectors in the body-fixed coordinate system are as follows:

$$f_G^o = \mathrm{J}_1^{-1}\begin{bmatrix}0\\0\\G^o\end{bmatrix}, \quad f_B^o = \mathrm{J}_1^{-1}\begin{bmatrix}0\\0\\B^o\end{bmatrix},$$
$$f_G^{\mathrm{F}} = \mathrm{J}_1^{-1}\begin{bmatrix}0\\0\\G^F\end{bmatrix}, \quad f_B^F = \mathrm{J}_1^{-1}\begin{bmatrix}0\\0\\B^F\end{bmatrix}$$

The torque $\mathrm{M}^o = r_{\mathrm{G}}^o \times f_G^o - r_B^o \times f_B^o$, $\mathrm{M}^F = r_{\mathrm{G}}^F \times f_G^{\mathrm{F}} - r_B^F \times f_B^F$. The restoring force and moment vector in the body-fixed coordinate system is as follows:

$$\mathrm{g}(\eta) = \begin{bmatrix}0\\0\\-r_x^W G_o C\theta^0 S\phi^0 - r_y^W G_o S\theta^0\\0\\0\\-r_x^B G_F C\theta^F S\phi^F - r_y^B G_F S\theta^F\end{bmatrix} \tag{16}$$

The part above the sea level is smaller compare to the total system. Disturbance forces like wind forces and wave forces are neglected in this paper. Thus, the inputs include the thrust generated by the glider wings at the bottom and the force due to the rudder angle δ. The control input vector τ can be expressed as follows:

$$\tau = \begin{bmatrix}X_T^G + X_{u\delta}^G(\delta)\\Y_T^G + Y_{u\delta}^G(\delta)\\N_{uu\delta}^G\\0\\0\\0\end{bmatrix} \tag{17}$$

The calculation method of the coefficients in the above formula will be described in section 3.

The full 6-DOF set of nonlinear model is obtained by substituting (5), (10)-(12) and (16)-(17) into equation (4), as (18), as shown at the bottom of the next page:

III. STRUCTURE EVALUATION OF WAVE GLIDER

A wave glider structure was designed for the boat with the size of 230 cm $*$ 80 cm$*$ 20 cm. The requirements for the designed glider structure are shown in Table 1.

TABLE 1. Requirement for glider wing.

Requirement	Value
Navigational speed	0.5 knot (0.2559 m/s)
Wave speed (vertical direction)	1 m/s

1) SIMPLIFIED EQUATIONS OF MOTION

The kinetic model of the wave glider is shown as equation (18) in Section 2. The horizontal drag force and the rudder angle are the only inputs of the model. When estimating the advance speed of the glider, we assume that the entire system moves in a line with rudder angle θ =0°, which means there is no deflection rudder angle for the rudder and the direction of the whole system will not be affected. The vertical displacement shall not be considered. The formula at X-axis is as follows:

$$(\mathrm{m}^0 - X_{\dot{u}}^G - X_{\dot{u}}^F)\dot{u}^0 + (-m^0 v^0 + Y_{\dot{v}}^0 v^0 + Y_{\dot{r}}^0 r^O)\mathrm{r}^0 + (X_u^F + X_u^G) = X_T^G + X_{u\delta}^G(\delta) \tag{19}$$

Formula (19) can be simplified to:

$$(\mathrm{m}^0 - X_{\dot{u}}^G - X_{\dot{u}}^F)\dot{u^0} + (X_u^F + X_u^G) = X_T^G \tag{20}$$

$X_{\dot{u}}^G, X_{\dot{u}}^F$ are added mass coefficient calculated by empirical formula:

$$\mathrm{X}_{\dot{u}}^{\mathrm{GF}} = \frac{m^{GF}}{100}[0.398 + 11.98C_b(1 + 3.73\frac{d}{B}) - (2.89C_b\frac{L}{B}) \times (1 + 1.13\frac{d}{B}) + 0.175C_b(\frac{L}{B})^2(1 + 0.541\frac{d}{B}) - 1.107\frac{L}{B}\frac{d}{B}] \tag{21}$$

where B is the width of the boat, L is the length of the boat, d is the mean draught, C_b is the block coefficient of the boat, X_T^G is the total horizontal thrust. There are eight wings for the Glider. The interaction between the surface floater and the Glider wings below is neglected. The total horizontal force of the Glider is $X_T^G = 8L$; horizontal drag force of a single blade is calculated by the mean value of the simulated results and the calculated results of different angles in this section.

$$\int_0^t \dot{u^0}\mathrm{dt} = \int_0^t (\frac{X_T^G - (X_u^F + X_u^G)}{(\mathrm{m}^0 - X_{\dot{u}}^G - X_{\dot{u}}^F)})\mathrm{dt} \tag{22}$$

Where t is estimated 5 seconds and u_t^0 =0.2559 m/s, u_0^0 =0 m/s. Total mass m^0 includes the weight of the floater, the glider wings, the dry box and the tether. The floater material is polypropylene with the density of 0.91 g/cm^3, the weight of the sensor of 5 kg, and the total mass of 80.3 kg. The other parameters are shown in Table 2.

$$X_T^G = 8\mathrm{L} = 226.7\mathrm{N}, \quad \mathrm{L} = \frac{1}{8}X_T^G = 28.35\mathrm{N}$$

TABLE 2. Estimated coefficient values.

Coefficient	Value
$\mathbf{X_u^F}$	37.2kg/m
$\mathbf{X_u^G}$	83.1kg/m
$\mathbf{X_{\dot{u}}^G}$	-1.72kg
$\mathbf{X_{\dot{u}}^F}$	-0.91kg
$\boldsymbol{\rho}$	1000kg/m^3
$\mathbf{m^0}$	80.3kg
$\mathbf{c_L}$	1.13
$\mathbf{S_{fin}}$	0.16m^2

2) DESIGNING OF GLIDER BLADE STRUCTURE

In order to design the required glider wing area, we analyses the static situation of a single glider wing. The glider wings convert vertical wave-induced flow to horizontal thrust. The force situation of the glider wings to derive the speed was analyzed. Hydrofoils, rudders, propeller blades are devise examples of lifting surfaces. Generally these are thin streamlined bodies, intended to develop a hydrodynamic lift force L. A single glider wing is approximated as a piece of hydrofoil. The performance of hydrofoil in water is analogous to that of airplane wing, and the principal distinction between these is the density of the fluid medium. Hydrofoil also experiences a drag force D. In a reference body-fixed with the hydrofoil, the drag component is in the same direction as the free stream, as shown in Fig. 3.

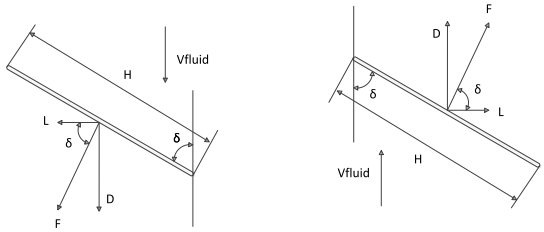

FIGURE 3. Schematic of load-carrying capability of glider blades.

The load-carrying capability of underwater glider's wings is derived using the equivalent lift force equation. Assume that the vertical wave-induced flow is in a constant speed and fixed angle of attack in an unbounded fluid, and that the ambient pressure is sufficiently high to preclude cavitation, similar with the force situation in the air, the force situation of the wings under water is simplified to horizontal force L and vertical force D [25], [26], as shown in Fig. 3.

$$
\begin{bmatrix}
\mathrm{m}^0 - X_{\dot{u}}^G - X_{\dot{u}}^F & 0 & 0 & 0 & 0 & 0 \\
0 & \mathrm{m}^0 - Y_{\dot{v}}^G - Y_{\dot{v}}^F & -Y_{\dot{r}}^G - Y_{\dot{r}}^F & 0 & 0 & 0 \\
0 & -N_{\dot{v}}^0 & I_{zz}^0 - N_{\dot{r}}^0 & 0 & 0 & 0 \\
0 & 0 & 0 & \mathrm{m}^F - X_{\dot{u}}^F & 0 & 0 \\
0 & 0 & 0 & 0 & \mathrm{m}^F - Y_{\dot{v}}^F & -Y_{\dot{r}}^F \\
0 & 0 & 0 & 0 & -N_{\dot{v}}^F & I_{zz}^F - N_{\dot{r}}^F
\end{bmatrix}
\begin{bmatrix} \dot{u}^0 \\ \dot{v}^0 \\ \dot{r}^0 \\ \dot{u}^F \\ \dot{v}^F \\ \dot{r}^F \end{bmatrix}
$$

$$
+ \begin{bmatrix}
0 & 0 & -\mathrm{m}^0 v^0 + Y_{\dot{v}}^O v^O & 0 & 0 & 0 \\
 & & Y_{\dot{r}}^O r^O & & & \\
0 & 0 & \mathrm{m}^0 u^0 - X_{\dot{u}}^O u^O & 0 & 0 & 0 \\
\mathrm{m}^0 v^0 - Y_{\dot{v}}^O v^O & -\mathrm{m}^0 u^0 + X_{\dot{u}}^O u^O & 0 & 0 & 0 & 0 \\
-Y_{\dot{r}}^O r^O & & & & & \\
0 & 0 & 0 & 0 & 0 & -\mathrm{m}^F v^F + Y_{\dot{v}}^F v^F + Y_{\dot{r}}^F \\
0 & 0 & 0 & 0 & 0 & \mathrm{m}^F u^F - X_{\dot{u}}^F u^F \\
0 & 0 & 0 & \mathrm{m}^F v^F - Y_{\dot{v}}^F v^F - Y_{\dot{r}}^F r^F & -\mathrm{m}^F u^F + X_{\dot{u}}^F u^F & 0
\end{bmatrix}
$$

$$
\times \begin{bmatrix} u^0 \\ v^0 \\ \mathrm{r}^0 \\ u^F \\ v^F \\ r^F \end{bmatrix}
- \begin{bmatrix} X_u^F + X_u^G \\ Y_v^F + Y_v^G \\ N_r^F + N_r^G \\ X_u^F + X_v^F \\ Y_u^F + Y_v^F \\ N_v^F + N_r^F \end{bmatrix}
+ \begin{bmatrix} 0 \\ 0 \\ -r_x^W G_o C\theta^0 S\phi^0 - r_y^W G_o S\theta^0 \\ 0 \\ 0 \\ -r_x^B G_F C\theta^F S\phi^F - r_y^B G_F S\theta^F \end{bmatrix}
= \begin{bmatrix} X_T^G + X_{u\delta}^G(\delta) \\ Y_T^G + Y_{u\delta}^G(\delta) \\ N_{uu\delta}^G \\ 0 \\ 0 \\ 0 \end{bmatrix}
\tag{18}
$$

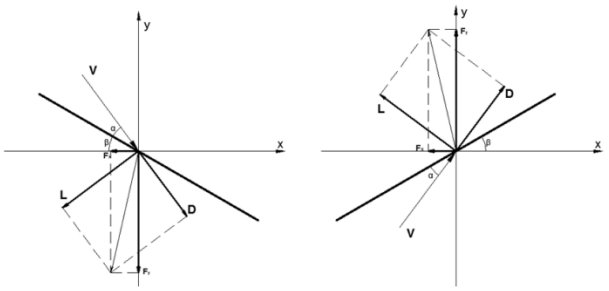

FIGURE 4. Wing stress analysis.

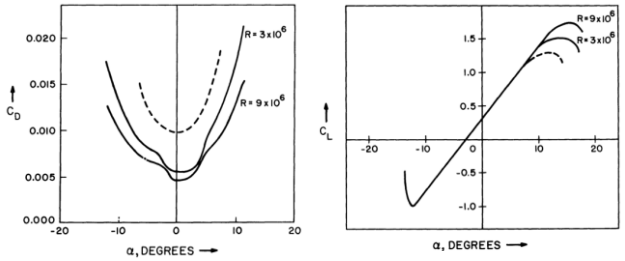

FIGURE 5. Drag coefficients and lift coefficients for the NACA 63-412 section [25].

When the wing is rising (descending), the stress analysis are shown in the left (right), as show in Fig 4. The horizontal component force is calculated as:

$$F_x = \mathrm{L}\sin(\alpha+\beta) - \mathrm{D}\cos(\alpha+\beta) \tag{23}$$

The angle of attack δ_e is generally defined foil deformation with respect to the ''nose-tail line'', i.e., the center of the minimum radius of curvature of the leading edge and the sharp trailing edge. The total force F is divided into horizontal component F_x and vertical componentF_y, which are defined respectively to be perpendicular and parallel to the X-axis. Following [24] and [25], L and D are calculated as:

Lifting force:

$$\mathrm{L} = \frac{1}{2}\rho c_L(\delta_e) S_{fin} v_{fluid}^2 \tag{24}$$

Drag force:

$$\mathrm{D} = \frac{1}{2}\rho c_D(\delta_e) S_{fin} v_{fluid}^2 \tag{25}$$

Substitute eq. (24) and (25) into (23), F_x and F_y are calculated as:

$$F_x = \frac{1}{2}\rho S_{fin} v_{fluid}^2 [c_L \sin(\alpha+\beta) - c_\mathrm{D}\cos(\alpha+\beta)] \tag{26}$$

$$F_y = \frac{1}{2}\rho S_{fin} v_{fluid}^2 [c_L \sin(\alpha+\beta) + c_\mathrm{D}\cos(\alpha+\beta)] \tag{27}$$

Where ρ represents the liquid density, c_L and c_D respectively represent the lift coefficient and the drag coefficient respectively, δ_e represents the angle of attack. The adopted NACA 63-412 foil section empirical curve for lift and drag coefficient estimation is shown in Fig. 5 and the blade nose-tail line with the specific parameter values shown in Table 2. Consequently the derived formulas are as follows:

TABLE 3. Calculation parameters.

Parameter	Value
L	1 m
ρ	1000 kg/m^3
S_{fin}	$S_0\cos\delta$
v_{fluid}	0.5m/s, 1m/s, 2m/s
δ	5°、10°、20°、30°、45°、60°

$$S_{fin} = \frac{2L}{\rho c_L(\delta_e) v_{fluid}^2} \tag{28}$$

$$S_0 = \frac{S_{fin}}{\cos\delta} = \frac{1}{5}\sum_{\delta_1}^{\delta_6} \frac{S_{fin}(\delta)}{\cos\delta} \tag{29}$$

v_{fluid} = 1m/s, consequently S_0 =0.21m^2

In this example, Reynolds number Re = ρvL/μ, ρ is the liquid density, v is the flow speed, and L is the fin length. When the flow goes vertically downward to the wings, the locking mechanism locks the wings after reaching the limiting constrained angle. After that the wings will be rotated back to the original position by the torsional spring. The lift forces of the wings were calculated with angles of attack deflected at 5°, 10°, 20°, 30°, 45°, 60°, respectively as well as the flow rates at 0.5 m/s, 1m/s, 2m/s. The section of the glider wing as a NACA 63-412 section was evaluated get c_L, c_D from Fig. 5. Other parameters are in Table 3.

3) SIMULATION OF HYDROFOIL ROTATION ANGLE

In order to estimate the range of rotation angle, the force situation of a single wing in fixed angle. The simulation is made at different angles when the flow rate is 0.5 m/s, 1 m/s, 2 m/s to compare the horizontal forces. The determined wing area in simulation is 0.21 m^2. The calculation results were carried out by using formula in the Section 3.2. The simulation curve and calculation were fitted to compare the force situation.

The comparison of the simulation results and the calculated value of the horizontal drag force are shown in Fig.6. Simulation results are shown in left, and the calculated value is shown in right. X-axis denotes the wing angle from 0° to 60°, Y-axis denotes the flow rate of 0.5 m/s, 1 m/s, 2 m/s respectively. It can be seen from the data that both

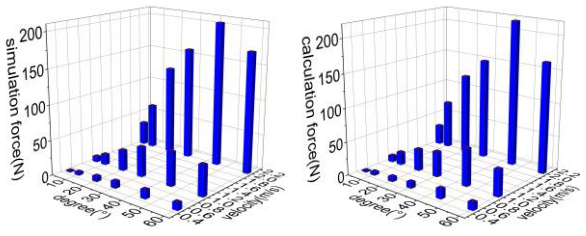

FIGURE 6. Drag force result contrastive analysis diagram.

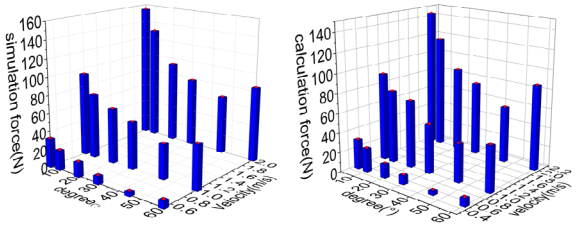

FIGURE 8. Lift force results contrastive analysis diagram.

TABLE 4. Horizontal drag force (V = 1 m/s).

Angle	Calculated value（N）	Simulation（N）
5°	1.94	7.692
10°	4.92	15.11
20°	6.89	29.698
30°	8.91	42.92
45°	14.54	48.84
60°	11.24	43.97

TABLE 5. Vertical lift force (V = 1 m/s).

Angle	Calculated value（N）	Simulation（N）
5°	90.64	93.57
10°	74.68	72.99
20°	69.36	62.13
30°	50.57	53.17
45°	39.31	39.24
60°	46.72	49.77

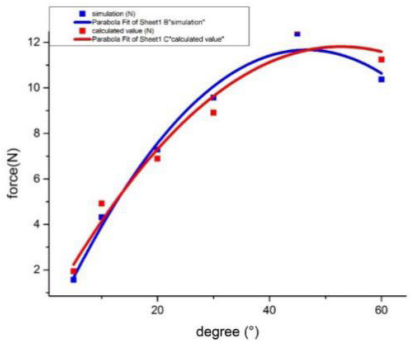

FIGURE 7. Fitting curve for degree to horizontal drag force.

the simulation horizontal component force and the calculation horizontal component force gradually increase as the angle of attack increases under the same flow rate. Both the simulation horizontal component force and the calculation horizontal component force gradually increase as the flow rate increases under the same angle of attack. The horizontal component force reaches the maximum value when the angle of attack reaches 45°. After that the horizontal component force decreasing as the angle of attack increases. The growth trend of the simulation is consistent with that of the calculation.

Horizontal drag force at V = 1 m/s obtained from calculation and simulation, as shown in table 4.

When V = 1 m/s, the parabolic method was adopted to fit curve for degree, as show in Fig. 7. By replacing the actual curve in the sector with parabola approximately, the fitting precision is highly improved compared with the linear interpolation. The fitted equation for simulation curve is as follows:

$$F_S1 = -0.88998 + 0.53821\delta - 0.00577\delta^2 \quad (30)$$

Where Fs reaches the maximum value at $\delta = 46.64°$.
The fitted equation for calculation curve is as follows:

$$Fc1 = 0.12279 + 0.44286\delta - 0.0042\delta^2 \quad (31)$$

Where Fc reaches the maximum value at $\delta = 52.72°$.

The comparison of the simulation results and the calculated value of the vertical lift force are shown in Fig. 8. The simulation result is shown in left, and the calculation value is shown in right. X-axis denotes the wing angle from 0° to 60°, Y-axis denotes the flow rate of 0.5 m/s, 1 m/s, 2 m/s respectively. It can be seen from the data in the above figure that both the simulation vertical component force and the calculation vertical component force gradually decrease as the angle of attack increases under the same flow rate. Both the simulation vertical component force and the calculation vertical component force gradually increase as the flow rate increases under the same angle of attack. The vertical component force reaches the minimum value when the angle of attack reaches 45°. After that the vertical component force increases as the angle of attack increases. The growth trend of simulation is corresponding to that calculated.

Vertical lift force at V = 1 m/s obtained from calculation and simulation, as shown in table 5.

When V = 1 m/s, the parabolic method was adopted to fit curve for degree, as show in Fig 9. By replacing the actual curve in the sector with parabola approximately, the fitting precision is highly improved compared with the linear interpolation. The empirical expression for simulation curve is as

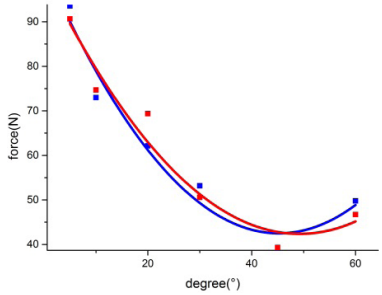

FIGURE 9. Fitting curve for degree to vertical lift force.

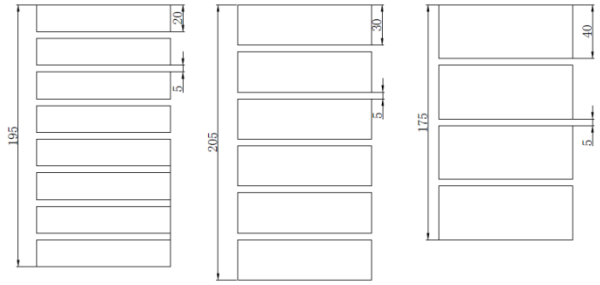

FIGURE 10. Wing array dimension chart.

follows:

$$Fs2 = 37.62783 - 1.43141\delta + 0.01575\delta^2 \quad (32)$$

Where Fs reaching the minimum value at $\delta = 45.44°$.

The calculation value is as follows:

$$Fc2 = 42.99271 - 1.70702\delta + 0.01933\delta^2 \quad (33)$$

Where Fc reaching the minimum value at $\delta = 44.15°$.

The main function of the wing is to convert the wave energy to tow the whole system. But on the other hand the wing should not pull the boat too deep to affect the solar panel system. The horizontal drag force increases as the wing angle increases from 0° to 45°. After that the horizontal drag force decreases and the vertical lift force increases. We choose 45° as maximum angle taking the simulation curve equation and calculation curve equation into consideration. When the wing angle is reaching 45°, the locking device will stop the rotate axis.

4) DIMENSION ANALYSIS OF HYDROFOIL BLADE

Glider wings array are arranged in parallel. There is a space between two wings, which will affect the flow field around. To compare the horizontal drag force with different number of wings at the same effective cross-sectional area, fins of 8-wing structure, 6-wing structure, and 4-wing structure were adopted to simulate respectively. The total force is shown in Fig.11. The other parameters of the blades are shown in Table 6. The simulation values and the theoretical calculated values are shown in Fig. 11.

Fig. 11 (a) shows the horizontal drag force at the same effective cross-sectional area S_{fin} with different hydrofoil widths at 20 cm, 30 cm, and 40 cm respectively. The same effective cross-sectional area S_{fin} is 160 cm ×100 cm.

Fig. 11 (b) is the ratio of the simulated horizontal drag force to the calculated value. The Fig. 10 shows that when the effective area is the same, the ratio of the simulation values to the calculated values is smaller and smaller as the hydrofoil width increases. When the width is 20 cm, the loss caused by the gap is the smallest, and the error between the simulated values and the calculated values is the minimum. Hence, 20 cm was adopted as the width of the wing.

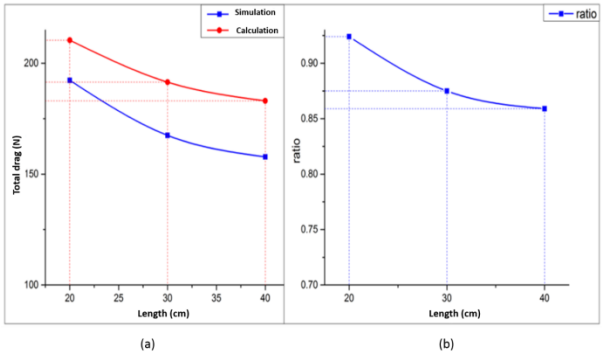

FIGURE 11. Hydrofoil dimension comparison.

TABLE 6. Wing parameters.

Parameter	Value
Effective cross-sectional area S_{fin}	160 cm×100 cm
δ	45°
v_{fluid}	1 m/s
Thickness	0.6 cm
Blade spacing	5 cm

IV. CONCLUTION REMARKS AND FUTURE WORK

In this paper we present a nonlinear 6-DOF kinetic model of the wave glider with a two-body structure. Kinetic model of other waterborne unmanned vehicle with monomer structure cannot accurately describe the motion parameters of the wave glider. The movement in waves of the glider with catamaran structure can be more accurately described by establishing a kinetic model with a two-body structure, which improves the shortcomings of the existing models.

In this paper, some influence factors on the horizontal drag force were estimated by comparing simulation and

calculation results. An equation of vertical flow speed and advance speed are derived by simplifying the kinetic model. Through the static analysis of glider wing, the deduced optimized wing area is determined and constrained by the simplified equations of motion to meet the speed requirement. By fitting the curve between degree and force, different rotation angles are compared to optimize the wing structure.

Some parameters have been simplified during the modeling process. The model is only suitable for those bodies with symmetric structure in vertical plane. The model needs to be modified if the structure of the wave glider changes. As the model does not consider the wave and the wind or other environment disturbances, it cannot accurately describe the movement in a more complex environment. The future work includes a sea test of the wave glider to optimize the structure to improve its stability. The lift and drag coefficients in field experiments will be carried out to compare with calculation and simulation results, as well as the interaction between the floater and the glider by measuring the azimuth angle. Sophisticated real-time motion simulation of wave glider in different sea state will be studied for best performance and applications.

CONFLICTS OF INTEREST

The authors declare no conflict of interest.

REFERENCES

[1] J. E. Manley, "Development of the autonomous surface craft 'ACES,'" in *Proc. MTS/IEEE Conf. OCEANS*, vol. 2, Oct. 1997, pp. 827–832.

[2] J. E. Manley, "Unmanned surface vehicles, 15 years of development," in *Proc. IEEE OCEANS*, Sep. 2008, pp. 1–4.

[3] T. W. Rochholz, "Wave-powered unmanned surface vehicle as a station-keeping gateway node for undersea distributed networks," Ph.D. dissertation, Naval Postgraduate School, Monterey, CA, USA, 2012.

[4] Y. Wang, A. Anvar, and E. Hu, "A feasibility study on the design, development and operation of an automated oceanic wave surface glider robot," in *Proc. 20th Int. Congr. Modelling Simulation Soc. Autralia New Zealand*, 2013, pp. 970–976.

[5] B. Bingham *et al.*, "Passive and active acoustics using an autonomous wave glider," *J. Field Robot.*, vol. 29, no. 6, pp. 911–923, 2012.

[6] C. D. Chadwell, "GPS-acoustic seafloor geodesy using a wave glider," in *Proc. AGU Fall Meeting Abstr.*, vol. 1, 2013, p. 1.

[7] J. E. Manley and G. Hine, "Unmanned surface vessels (USVs) as tow platforms: Wave glider experience and results," in *Proc. IEEE Oceans*, Sep. 2016, pp. 1–5.

[8] V. Van Lancker and M. Baeye, "Wave glider monitoring of sediment transport and dredge plumes in a shallow marine sandbank environment," *PLoS ONE*, vol. 10, no. 6, p. e0128948, 2015.

[9] M. A. Benson *et al.*, "Acquisition using autonomous marine vehicles: Wave glider field test, offshore Abu Dhabi," in *Proc. SPE Middle East Oil Gas Show Conf.*, 2017, pp. 1–9.

[10] W. Al-Sabban, J. Das, and R. N. Smith, "Persistent robot tasking for environmental monitoring through crowd-sourcing," in *Proc. IEEE Oceans*, San Diego, CA, USA, Sep. 2014, pp. 1–6.

[11] A. Caiti, V. Calabrò, S. Grammatico, A. Munafò, and M. Stifani, "Lagrangian modeling of the underwater wave glider," in *Proc. IEEE Oceans*, Jun. 2011, pp. 1–6.

[12] X. T. Li, F. Liu, L. Wang, and H-Q. She, "Motion analysis of wave glider based on multibody dynamic theory," in *Intelligent Robotics and Applications*. Cham, Switzerland: Springer, 2017, pp. 721–734.

[13] T. T. J. Prestero, "Development of a six-degree of freedom simulation model for the REMUS autonomous underwater vehicle," in *Proc. MTS/IEEE Oceans Ocean Odyssey Conf.* Cambridge, CA, USA: Massachusetts Institute Of Technology, Nov. 2001, pp. 450–455.

[14] R. Hine and P. Mcgillivary, "Wave powered autonomous surface vessels as components of ocean observing systems," in *Proc. PACON*, Honolulu, HI, USA, 2007, pp. 1–9.

[15] J. Manley and G. Hine, "Persistent unmanned surface vehicles for subsea support," in *Proc. Offshore Technol. Conf.*, Houston, TX, USA, 2011, pp. 1–8.

[16] R. G. Burcham *et al.*, "Wave power," U.S. Patent 8 043 133, Oct. 25, 2011.

[17] T. Daniel, J. Manley, and N. Trenaman, "The wave glider: Enabling a new approach to persistent ocean observation and research," *Ocean Dyn.*, vol. 61, no. 10, pp. 1509–1520, 2011.

[18] C. H. Greene *et al.*, "A wave glider approach to fisheries acoustics: Transforming how we monitor the nation's commercial fisheries in the 21st century," *Oceanography*, vol. 27, no. 4, pp. 168–174, 2014.

[19] J. Manley and S. Willcox, "The wave glider: A new concept for deploying ocean instrumentation," *IEEE Instrum. Meas. Mag.*, vol. 13, no. 6, pp. 8–13, Dec. 2010.

[20] J. G. Graver, "Underwater gliders: Dynamics, control and design," *J. Fluids Eng.*, vol. 127, no. 3, pp. 523–528, 2005.

[21] T. I. Fossen, *Guidance and Control of Ocean Vehicles*. New York, NY, USA: Wiley, 1994.

[22] M. Ó'Catháin, B. J. Leira, J. V. Ringwood, and J.-C. Gilloteaux, "A modelling methodology for multi-body systems with application to wave-energy devices," *Ocean Eng.*, vol. 35, no. 13, pp. 1381–1387, 2008.

[23] M. S. Triantafyllou, "Maneuvering and control of surface and underwater vehicles," Massachusetts Inst. Technol., Cambridge, CA, USA, Tech. Rep., 2004.

[24] J. N. Newman, *Marine Hydrodynamics*, vol. 45, no. 2. Cambridge, MA, USA: MIT Press, 1977, p. 457.

[25] I. H. Abbott and A. E. von Doenhoff, *Theory of Wing Sections: Including a Summary of Airfoil Data*. New York, NY, USA: Dover, 1959.

[26] J. Denavit and R. S. Hartenberg, "A kinematic notation for lower-pair mechanisms based on matrices," *Trans. ASME J. Appl. Mech.*, vol. 22, no. 2, pp. 215–221, 1955.

Authors' photographs and biographies not available at the time of publication.